Check for updates

Received: 10 December 2022 | Revised: 19 February 2023 | Accepted: 13 March 2023

DOI: 10.1002/bio.4488

RESEARCH ARTICLE

LUMINESCENCE The Journal of Biological and Chemical Luminescence WILEY

Zinc silicate phosphor: Insights of X-ray induced and temperature enabled luminescence

P. Diana[1] | Subramanian Saravanakumar[1] | D. Sivaganesh[1,2] | V. Sivakumar[3] | Yang Li[4] | S. Sebastian[5] | Ji-Man Kim[6] | Padmanathan Karthick Kannan[6] | L. Sangeetha[7] | Vijayendran K. K. Praneeth[8]

[1]Department of Physics, Kalasalingam Academy of Research and Education, Krishnan Koil, Tamil Nadu, India

[2]Ural Federal University, Mira str., Yekaterinburg, Russia

[3]Department of Physics, M. Kumarasamy College of Engineering, Karur, Tamil Nadu, India

[4]School of Biomedical Engineering, Guangzhou Medical University, Guangzhou, Guangdong, China

[5]Department of Physics, Arul Anandar College, Karumathur, Madurai, Tamil Nadu, India

[6]Department of Chemistry, Sungkyunkwan University, Suwon, The Republic of Korea

[7]Department of Physics, Saveetha Engineering College, Chennai, Tamil Nadu, India

[8]Department of Chemistry, Kalasalingam Academy of Research and Education, Krishnan Koil, Tamil Nadu, India

Correspondence
Subramanian Saravanakumar, Department of Physics, Kalasalingam Academy of Research and Education, Krishnan Koil 626 126, Tamil Nadu, India.
Email: saravanaphysics@gmail.com

Padmanathan Karthick Kannan, Department of Chemistry, Sungkyunkwan University, 2066, Seobu-ro, Jangan-gu, Suwon-Si 16419, Gyeonggi-do, South Korea.
Email: pkk.matsci@gmail.com

Abstract

The present investigation deals with the effect of calcination temperature on the structural and thermoluminescent (TL) properties of Zn_2SiO_4 materials. For this study, Zn_2SiO_4 was prepared via a simple hydrothermal route and calcinated at temperatures from 700°C to 1100°C in an air atmosphere. TL data of all Zn_2SiO_4 samples showed two peaks at around 240°C and 330°C due to the formation of the luminescence centre during X-ray irradiation. More interestingly, the Zn_2SiO_4 sample calcinated at 900°C exhibited a shift in the TL peak (282°C and 354°C) with an optimal TL intensity attributed to its good crystallinity with a well-defined hexagonal plate-like morphology. X-ray-irradiated Zn_2SiO_4 samples calcinated at 900°C exhibited a high-temperature TL glow curve peak, suggesting that the present material could be used for high-temperature dosimetry applications.

KEYWORDS
dosimetry applications, Rietveld refinement, thermoluminescence, Zn_2SiO_4

1 | INTRODUCTION

Over the past few decades, high-energy ionizing radiation such as gamma rays, X-rays and ultraviolet (UV) rays has been widely used in various applications in the science and engineering fields. The effectiveness of high-energy ionizing radiation instantly impacts humankind, which affects cell tissues and deoxyribonucleic acid (DNA), leading to permanent human disorders. Therefore, sensing and monitoring radiation levels are essential for protecting humans exposed to radiation [1]. This type of radiation is not visible, so people cannot generally sense its presence [2]. Various techniques, such as scintillators, counters, photoresists, and solid-state detectors (i.e., thermoluminescent dosimeters), are available for the detection and measurement of high-energy ionizing radiation. Radiation dosimetry detects and measures ionizing radiation based on the thermoluminescence (TL). It is widely used due to its high sensitivity, accuracy, and simplicity [3]. Thermoluminescence is a well known light emission process that occurs when a substance is heated after absorbing

 © 2023 John Wiley & Sons Ltd.

radiation [4]. Radiation dosimetry estimates the ageing of inorganic materials and investigates kinetic parameters and defects. In TL dosimeters (TLDs), a trapped state is formed when radiation reaches the material. Then, when the material is heated, light energy is emitted that can be observed as a TL glow curve. The TL properties of a material can be derived from the glow peak position, shape, and intensity of the TL glow curve.

Material energy transfer mechanisms and trapped states/charges have been studied based on their TL glow peaks [5–7]. The TL glow peaks emitted by phosphor are used to estimate kinetic parameters such as order of kinetics (b), frequency factor(s), and activation energy (E) for dosimetric applications [8, 9]. The main advantage of TLD is its compactness and the fact that no cables or auxiliary devices are required during dose measurement. It is widely used in high-dose ionizing radiation dosimetry, for dating archaeological specimens, forensic experimentations, food dosimetry, radiation therapy, mapping of cancer cells, and nuclear medicine.

Various phosphors have been investigated based on the TL properties for use as detectors and dosimeters. Zn_2SiO_4 phosphor has attracted much attention due to its multifunctionality and marked properties, such as high luminescence efficacy, highly stable structure, and high band gap (~5.5 eV) [10, 11].

The most common thermoluminescent materials used for radiation dosimetry are LiF:Mg,Ti, $CaSO_4$:Dy, $CaSO_4$:Tm, Al_2O_3:C, etc. Many reports have described using rare earth ions and transition metal ion-doped Zn_2SiO_4 materials for optoelectronics applications. However, the TL behaviour of Zn_2SiO_4 is yet to be reported. The TL properties of undoped willemite (Zn_2SiO_4) minerals were described by T.K.G. Rao [12], who said that the prepared material exhibited five peaks at 160°C, 225°C, 260°C, 310°C, and 400°C during γ-ray irradiation; the corresponding defect centre was confirmed using electron paramagnetic resonance (EPR). Pontsho Mbule et al. recently prepared a Dy^{3+}-doped Zn_2SiO_4 nanophosphor using a sol–gel approach and investigated its TL properties [13], three TL glow peaks at 90, 180, and 375°C were obtained after beta-source irradiation. The estimated activation energies of the electrons were in reasonably good agreement. Experimental evidence suggests that Dy^{3+}-doped Zn_2SiO_4 is a promising phosphor for dosimetry applications. Portakal-Uçar et al. investigated the TL properties of Ce^{3+} and Mn^{2+} co-activated Zn_2SiO_4 under X-ray irradiation [14]. They noted the improvement in TL performance of the Zn_2SiO_4:Ce phosphor. The effect of Sm^{3+} and Mn^{2+} incorporation into the structure and luminescence properties of Zn_2SiO_4 phosphor were also reported by Portakal-Uçar et al. [15]. The kinetic parameters of Zn_2SiO_4:Sm^{3+},Mn^{2+} were evaluated using various heating rates (VHR), initial rise (IR), and computerized glow curve deconvolution (CGCD) methods. They recommended that Sm and Mn incorporated into the Zn_2SiO_4 phosphor is a good candidate for use in TL dosimetry.

Several researchers have devised numerous techniques for Zn_2SiO_4 synthesis including the sol–gel [16], sonochemical [17], polymer precursor [18], and spray pyrolysis methods [19], as well as solid-state reactions [20], and hydrothermal synthesis routes [21]. Interestingly, hydrothermal synthesis has many advantages, including relatively gentle operating conditions, a single-step synthesis strategy, environmental friendliness, and fine dispersion in solution [22]. In addition to that, hydrothermal synthesis is inexpensive in terms of instrumentation, energy, and material precursors compared with other wet chemical methods [22]. Conversely, calcination temperature has a significant effect on the physicochemical properties of the prepared phosphor materials. During material synthesis, the calcination temperature causes crystallinity, morphological characteristics, atomic disorder, oxygen vacancy, and a segregated secondary phase, resulting in the improved optical and physical properties of the phosphor materials [23]. Following this idea, in the present work, a Zn_2SiO_4 phosphor was synthesized using a hydrothermal approach and prepared at various calcination temperatures for dosimetry applications.

2 | EXPERIMENTAL SECTION

2.1 | Materials

Here, 99% AR grade $Zn(NO_3)_2{\cdot}6H_2O$ (zinc nitrate hexahydrate purchased from LOBA), 99.5% AR grade SiO_2 nanopowder (silicon dioxide, purchased from Sisco Research Laboratories) and 98% of AR grade sodium hydroxide (NaOH pellets purchased from LOBA) were used as starting precursors and used as received.

2.2 | Sample preparation

Zn_2SiO_4 material was prepared using a hydrothermal method. Initially, 14.87 g of $Zn(NO_3)_2$ were dissolved in 100 ml of deionized (DI) water to make 1 M $Zn(NO_3)_2{\cdot}6H_2O$; 3.004 g of fumed SiO_2 powder was dissolved in DI water to make 1 M SiO_2. Then SiO_2 was added dropwise to the $Zn(NO_3)_2{\cdot}6H_2O$ solution under stirring. After that, the pH was adjusted to 11 using a NaOH solution. The colloidal solution was then transferred to an autoclave and heated at 180°C for 12 h. Afterwards, the sample was centrifuged and dried at 70°C for 12 h. The dried sample was then calcinated at various temperatures such as 700°C, 800°C, 900°C, 1000°C, and 1100°C for 2 h using a muffle furnace. The calcinated Zn_2SiO_4 powder was characterized further. The preparation process for Zn_2SiO_4 is illustrated in Scheme 1.

2.3 | Sample characterization

The thermal stability of the dried Zn_2SiO_4 material was measured using a Netzsch TG-DSC thermal analyzer, and the data were obtained at room temperature to 1200°C at a heating rate of 10°C/min. The Zn_2SiO_4 samples calcinated at various temperatures were investigated using a powder X-ray diffractometer to identify their crystallinity by monochromatic CuK_α in the range 10–80° with a step size of 0.02°. The surface morphology of the sample was

15227243, 2023, 5, Downloaded from https://analyticalsciencejournals.onlinelibrary.wiley.com/doi/10.1002/bio.4488 by Sungkyunkwan University, Wiley Online Library on [16/08/2023]. See the Terms and Conditions (https://onlinelibrary.wiley.com/terms-and-conditions) on Wiley Online Library for rules of use; OA articles are governed by the applicable Creative Commons License

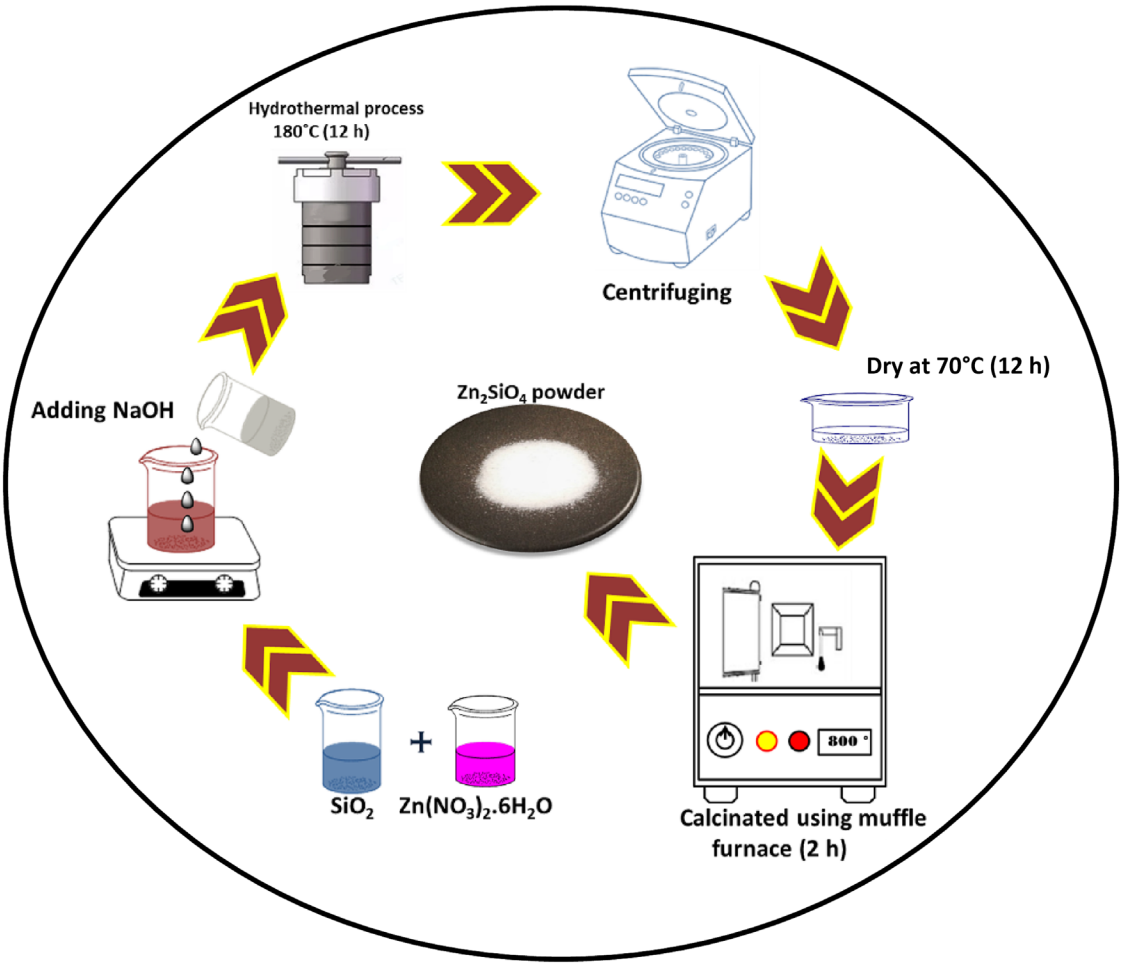

SCHEME 1 Preparation of the Zn_2SiO_4 material.

examined using scanning electron microscopy (SEM) (ZEISS-EVO 18 Research model), and the elemental purity of the Zn_2SiO_4 components was confirmed using energy dispersive X-ray spectroscopy (EDAX-APEX). The intramolecular and intermolecular vibrations of prepared Zn_2SiO_4 materials were investigated using a Raman spectrometer (BWS415-785S). The diffuse reflectance spectra (DRS) of all the synthesized Zn_2SiO_4 materials were recorded using a UV–visible DRS spectrophotometer (Shimadzu/UV 2600). The peak position and intensity of the TL glow peak were measured using a Nucleonix computer-based TL reader (type: TL 10091) at a linear heating rate of 8°C/s.

3 | RESULTS AND DISCUSSION

3.1 | Thermogravimetry differential thermal analysis (TG-DTA)

Figure 1 shows the TG and DTA profiles of the as-prepared Zn_2SiO_4 sample. The TG profile shows a significant weight loss between 50°C and 900°C due to the evaporation, decomposition and breakdown reactions of the prepared material [24]. In the temperature range 60–130°C, an exothermic peak was observed at 108°C that corresponded to an initial weight loss of Zn_2SiO_4 and due to the evaporation of residual solvent and water [25]. The second significant weight loss was caused by decomposition of zinc nitrate with an exothermic peak at 435°C, which resulted from the dehydroxylation of Si–OH into SiO_2 [25]. A third weight loss of Zn_2SiO_4 can occur between 630°C and 800°C, with an exothermic peak at 690°C [22] due to other residual compounds. No weight loss was observed after 780°C, attributed to the formation of crystalline Zn_2SiO_4 [25].

3.2 | Structural analysis

Powder X-ray diffraction (PXRD) analysis is used to determine the structural parameters of calcinated Zn_2SiO_4 materials. The phase pure rhombohedral structured α-Zn_2SiO_4 was identified in the prepared materials, and the diffraction peaks matched the standard JCPDS pattern well (card no. 37-1485) [26]. No additional peaks were identified in the observed diffraction patterns, indicating the high purity of the

15227243, 2023, 5, Downloaded from https://analyticalsciencejournals.onlinelibrary.wiley.com/doi/10.1002/bio.4488 by Sungkyunkwan University, Wiley Online Library on [16/08/2023]. See the Terms and Conditions (https://onlinelibrary.wiley.com/terms-and-conditions) on Wiley Online Library for rules of use; OA articles are governed by the applicable Creative Commons License

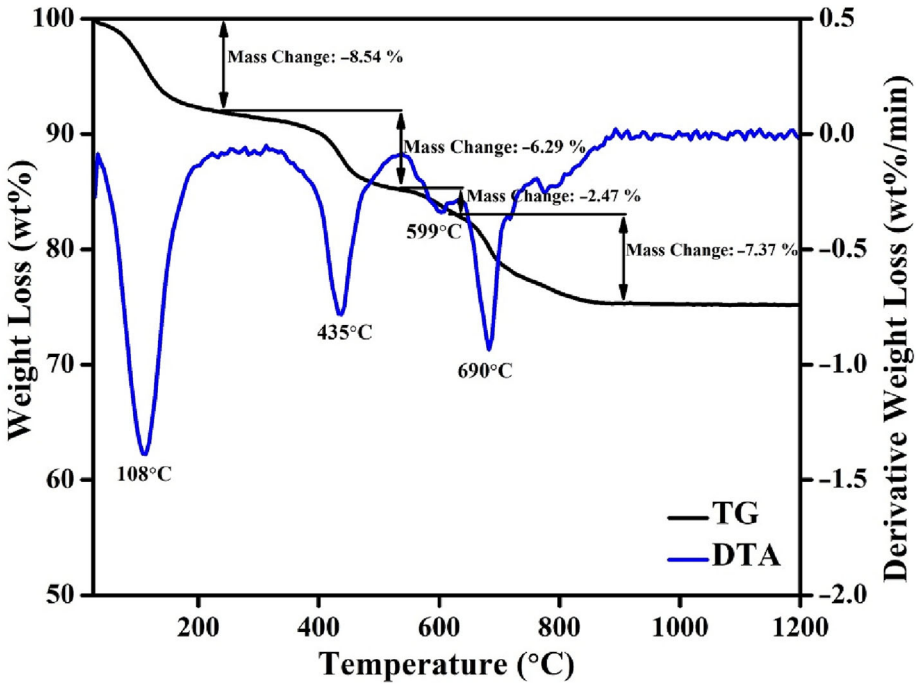

FIGURE 1 TG-DTA curves of the as-prepared Zn_2SiO_4 material.

synthesized materials, as shown in Figure 2a. With the increase in the calcination temperature from 700°C to 900°C, the diffraction peak shifted towards a higher angle side of 2θ (Figure 2b). Conversely, a shift in the diffraction angle towards the lower angle side of 2θ was observed for the samples calcinated at 1000°C and 1100°C. The changes in the diffraction angle shift are reflected in the cell constants shown in Table 1. The diffraction peak intensity gradually increased up to 900°C, revealing that increase in the calcination temperature improved the crystallization process [26, 27]. Further increases in the calcination temperatures, such as to 1000°C and 1100°C, lowered the diffraction peak intensity due to the lattice distortion in the host crystal structure [28]. Figure 2b shows that a higher diffraction peak intensity was obtained in the Zn_2SiO_4 material calcinated at 900°C, observing the lower full width at half maximum (FWHM) due to the presence of a larger crystallite size [27, 29]. Scherrer's equation [30] was used to determine the average crystallite size of the Zn_2SiO_4 materials. The average crystallite sizes of Zn_2SiO_4 calcinated at 700°C, 800°C, 900°C, 1000°C, and 1100°C were ~40, 48, 60, 54, and 51 nm, respectively. The sharp diffraction peak and smaller FWHM indicated a crystallization process improvement [29]. According to an earlier report, the diffusion rate of ions in the material increased at a specific calcination temperature, accelerating the crystal growth within the appropriate grain boundaries in the defined preferential orientation direction [31]. In the present study, the PXRD result suggested that a calcination temperature 900°C was preferable for Zn_2SiO_4 materials due to its high crystallinity. The lower and higher angle peak shifting of the observed X-ray profiles indicated that the synthesized materials underwent lattice strain due to the thermal treatment. Strain is an important parameter for measuring lattice constant distribution, such as lattice disorder due to crystal imperfection; strain was calculated as reported by Khorsand Zak et al. [29]. Table 2 shows the calculated strain values of all the prepared materials. The values show that the Zn_2SiO_4 material calcinated at 900°C had the lowest strain, indicating that the material had undergone a uniform distribution that led to maximum higher angle shifting (Figure 2b). As the calcination temperature was increased further, the Zn_2SiO_4 lattices experienced a higher strain, leading to a lower angle shifting, as shown in Figure 2b.

The Rietveld refinement technique [32–34] was used for the detailed structural analysis of the Zn_2SiO_4 phosphor, carried out using JANA 2006 software [35, 36]. The general Wyckoff's positions of Zn1 (0.9768, 0.1920, 0.0832), Zn2 (0.9768, 0.1913, 0.4173), Si (0.9836, 0.1952, 0.7529), O1 (0.1102, 0.2156, 0.7524), O2 (−0.0063, 0.3162, 0.7468), O3 (0.9189, 0.1256, 0.8901), and O4 (0.9251, 0.1973, 0.6014) for Zn_2SiO_4 were used for the refinement process [37]. Figure 3a–e shows the refined profiles of prepared materials. The small vertical blue line indicates the Bragg position in these figures. The horizontal green line represents the discrepancy between observed and calculated profiles. The precise fitting of the Rietveld profile again confirmed the phase pure system of the prepared materials. The refined structural parameters of the prepared Zn_2SiO_4 materials are tabulated in Table 1.

3.3 | Morphology analysis

The effect caused by thermal treatment in the morphology of Zn_2SiO_4 was examined using SEM analysis. Calcination temperature affected the material surface morphology. Figure 4a–e shows the SEM micrographs of the synthesized Zn_2SiO_4 materials calcinated at 700–1100°C. A highly agglomerated unclear hexagonal-shaped morphology was observed in the Zn_2SiO_4 materials calcinated at 700°C and

15227243, 2023, 5, Downloaded from https://analyticalsciencejournals.onlinelibrary.wiley.com/doi/10.1002/bio.4488 by Sungkyunkwan University, Wiley Online Library on [16/08/2023]. See the Terms and Conditions (https://onlinelibrary.wiley.com/terms-and-conditions) on Wiley Online Library for rules of use; OA articles are governed by the applicable Creative Commons License

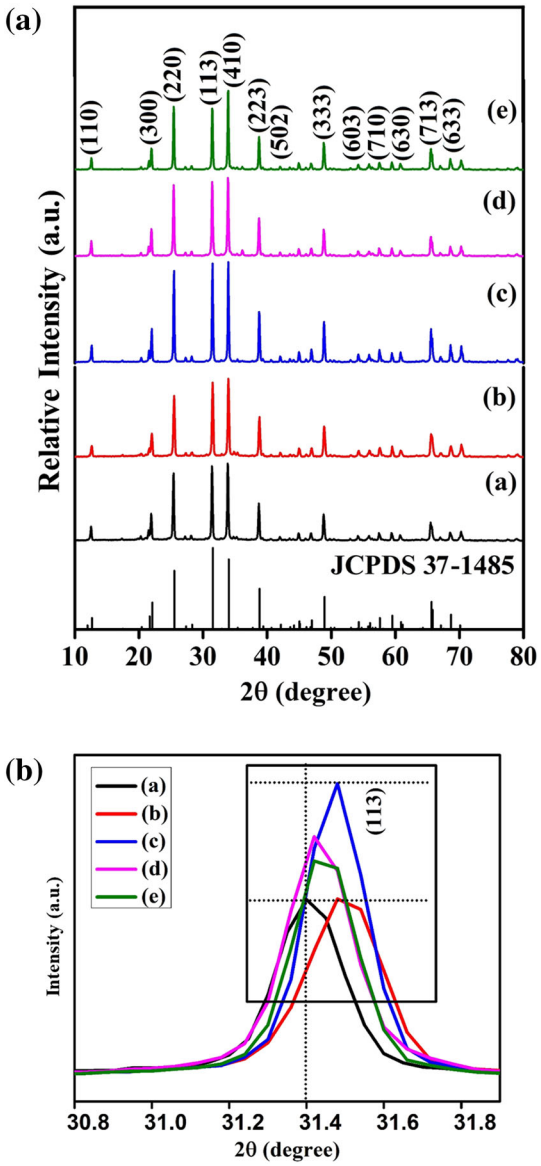

FIGURE 2 (a) Observed PXRD profiles of the Zn_2SiO_4 materials calcinated at (curve a) 700°C, (curve b) 800°C, (curve c) 900°C, (curve d) 1000°C, and (curve e) 1100°C. (b) Enlarged PXRD patterns on the (113) plane of the Zn_2SiO_4 materials calcinated at (curve a) 700°C, (curve b) 800°C, (curve c) 900°C, (curve d) 1000°C, and (curve e) 1100°C.

800°C. A very clear hexagonal-shaped morphology was observed in the Zn_2SiO_4 material calcinated at 900°C. A partially hexagonal-shaped morphology was observed in the Zn_2SiO_4 materials calcinated at 1000°C and 1100°C.

As shown Figure 4a,b, high agglomeration was observed at the low reaction temperature. As seen in the micrographs, at 700°C and 800°C calcinated temperature, more agglomerated nonhomogeneous particles were observed, whereas agglomeration was reduced, and homogeneity increased with increasing calcination temperature. A well dispersed and less agglomerated homogeneous hexagonal-shaped morphology was observed for Zn_2SiO_4 calcinated at 900°C. This may have been due to the surface diffusion during the calcination process that may have directed to high crystallinity (Figure 2b). As the calcination temperature was further increased to 1000°C and 1100°C, larger, irregular, and segregated particles were observed, possibly due to the higher temperature. This was because, as the crystal's degree of calcination was increased, morphology's destructiveness was augmented. It should be noted that calcination temperature was the most important factor for controlling the surface morphology of the materials.

The EDS study provided the elemental purity of the prepared Zn_2SiO_4 materials. No other elemental peaks were detected except for the Zn, Si, and O elements, as shown in Figure S1. This authenticated the purity of the synthesized material.

3.4 | Raman spectroscopy analysis

Raman spectroscopy was used to measure the changes in the molecular vibrations of Zn_2SiO_4 calcinated at various temperatures. In Figure 5, the Raman spectra for Zn_2SiO_4 calcinated at 700°C exposed substantial Raman scattering concentrated at 868, 904, and 944 cm^{-1} [38], all of which corresponded to siloxane groups. Furthermore, the molecular vibrations of Zn_2SiO_4 calcinated at 800°C, 900°C, 1000°C and 1100°C materials showed the same vibrations. No shift was observed in the Raman spectrum, as shown in Figure 5 (inset). The observed Raman spectra of Zn_2SiO_4 were comparable with the previous literature reports [38, 39]. Elghniji et al. [40] reported that the degree of crystallization strongly influenced the intensity of the Raman bands of the material. In the present work, the intensity of the

TABLE 1 Rietveld refinement parameters of the Zn_2SiO_4 materials.

	Calcination temperature (°C)				
Refined parameters	**700**	**800**	**900**	**1000**	**1100**
a = b (Å)	13.9998 (11)	13.9317 (8)	13.8861 (3)	13.9339 (9)	13.9404 (6)
c (Å)	9.3470 (9)	9.3026 (9)	9.2698 (5)	9.3042 (7)	9.3090 (3)
Volume ($Å^3$)	1586.52 (1)	1563.72 (1)	1547.99 (2)	1564.43 (4)	1566.754 (2)
Density (g/cm^3)	4.1	4.2	4.3	4.2	4.2
R_{obs} (%)	2.91	2.94	3.5	3.47	3.98
R_p (%)	5.41	5.68	6.46	6.87	7.06
GOF	1.36	1.53	1.68	1.56	1.61

15227243, 2023, 5, Downloaded from https://analyticalsciencejournals.onlinelibrary.wiley.com/doi/10.1002/bio.4488 by Sungkyunkwan University, Wiley Online Library on [16/08/2023]. See the Terms and Conditions (https://onlinelibrary.wiley.com/terms-and-conditions) on Wiley Online Library for rules of use; OA articles are governed by the applicable Creative Commons License

X-ray diffraction peaks increased gradually from 700°C to 900°C and then decreased, affecting the Raman band. In the observed Raman band, such as at 868, 904, and 944 cm^{-1}, a higher intensity was obtained for Zn_2SiO_4 calcinated at 900°C, which was due to the increased crystallinity observed in the chosen material.

TABLE 2 Lattice strain of the Zn_2SiO_4 materials.

Calcination temperature (°C)	Strain (ε) × 10^{-4}
700	47.50
800	47.14
900	32.40
1000	45.20
1100	45.27

3.5 | UV–Visible DRS analysis

The optical properties and band gap of the Zn_2SiO_4 materials were investigated using DRS. The reflectance spectra of the synthesized Zn_2SiO_4 materials are shown in Figure 6. The material's reflectance was less at short wavelengths up to 370 nm, indicating that the Zn_2SiO_4 matrix absorbed more electromagnetic radiation. The materials exhibit more reflectance at wavelengths of more than 370 nm. An absorption edge occurred between 370 and 800 nm [41]. The optical energy gap (E_g) was obtained using the Kubelka–Munk equation [42, 43], and the estimated E_g values were 5.35, 5.21, 5.18, 5.23, and 5.26 eV, respectively, as shown in Figure 7. The obtained band gap value was more analogous to findings detailed in a previous publication [39]. The variation in the bandgap energy with respect to temperature may have been caused by the presence of oxygen vacancies

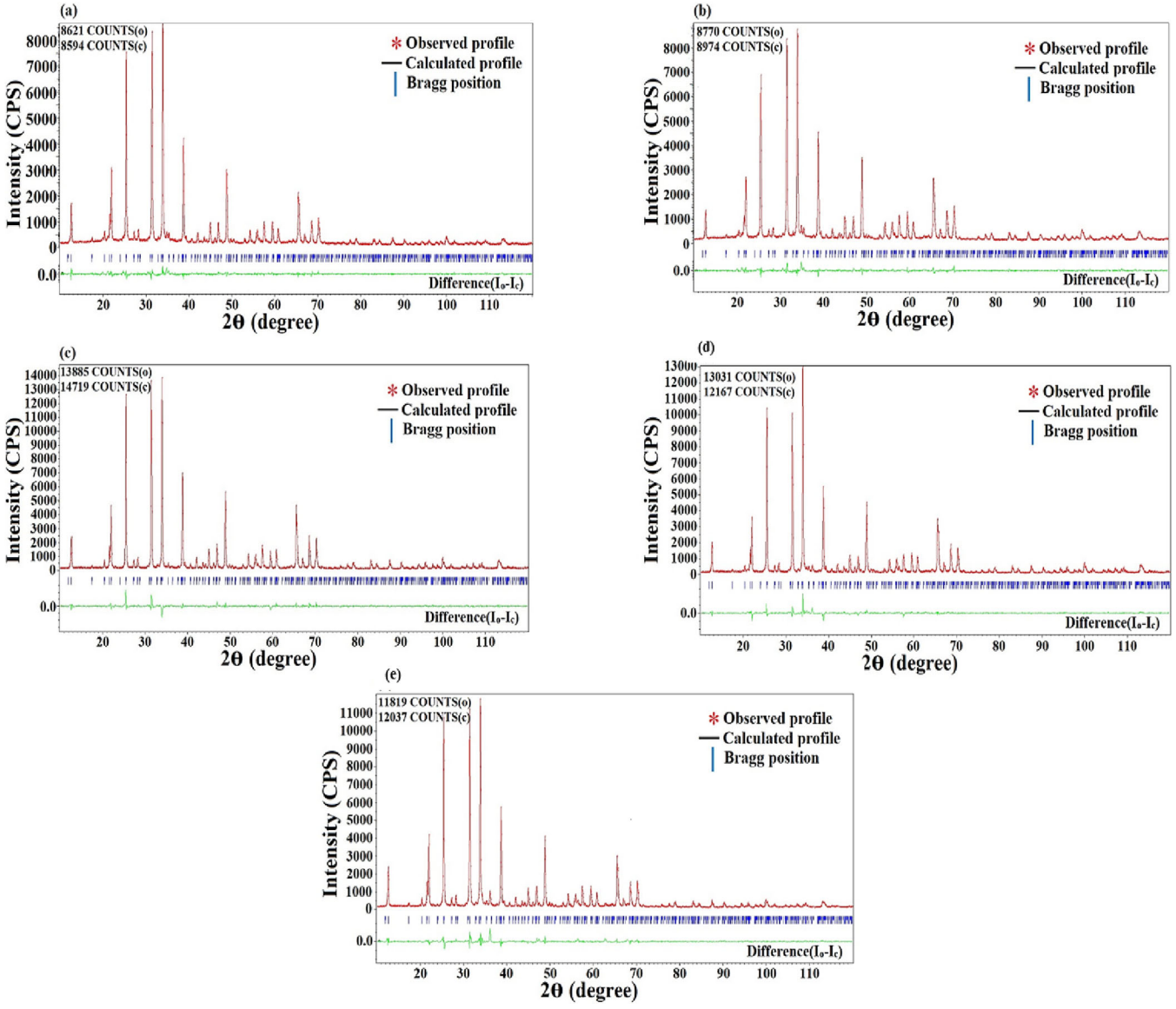

FIGURE 3 Rietveld refinement profiles of the Zn_2SiO_4 materials calcinated at (a) 700°C, (b) 800°C, (c) 900°C, (d) 1000°C, and (e) 1100°C.

15227243, 2023, 5, Downloaded from https://analyticalsciencejournals.onlinelibrary.wiley.com/doi/10.1002/bio.4488 by Sungkyunkwan University, Wiley Online Library on [16/08/2023]. See the Terms and Conditions (https://onlinelibrary.wiley.com/terms-and-conditions) on Wiley Online Library for rules of use; OA articles are governed by the applicable Creative Commons License

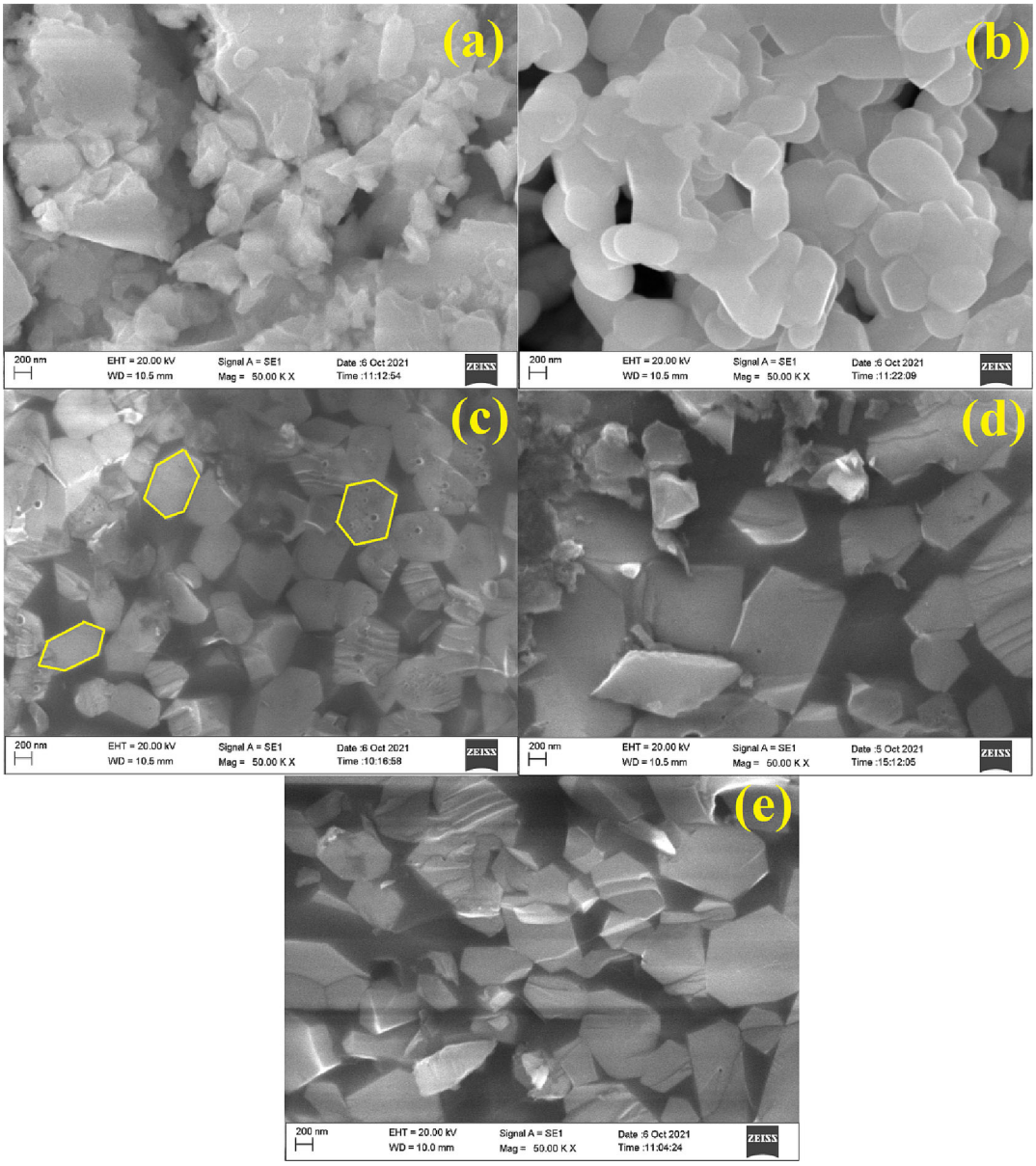

FIGURE 4 SEM micrographs of the Zn_2SiO_4 materials calcinated at (a) 700°C, (b) 800°C, (c) 900°C, (d) 1000°C, and (e) 1100°C.

[40]. The results revealed that Zn_2SiO_4 calcinated at 900°C possessed a lower energy gap (5.21 eV).

3.6 | Thermoluminescence (TL) analysis

The TL glow curve could be measured by heating the irradiated phosphor. The glow curve pattern, luminescence efficiency, and TL sensitivity were determined by its crystal nature and optimized by calcination temperature. The TL glow curve of Zn_2SiO_4 calcinated at various temperatures was recorded at a heating rate of 8°C/s after X-ray irradiation (0.57 Gy), as shown in Figure 8. Two distinct broad peaks appeared in all the prepared samples, one at low temperature (peak 1) of ~175–290°C with low intensity and another at a high intensity of ~295–400°C (peak 2). The peak positions of the TL glow curve are given in Table 3. The shift in the peak position was observed (see Figure 8) due to the change in the population of electron trapping centres or luminescence centres in the phosphor material [13]. The TL intensity increased linearly with calcination temperature, reaching a maximum intensity at 900°C and then decreased at 1000°C and 1100°C. The maximum TL intensity at 900°C was due to its high crystallinity and confirmed by X-ray diffraction (XRD) analysis. A high-temperature peak shift and higher peak intensity were observed in the Zn_2SiO_4 phosphor calcinated at 900°C due to the defect maintained in the Zn_2SiO_4 crystal lattice. The highly intense TL glow peak at high temperatures retained the deeper trap, with better stability, a slower rate of fading, and superior storage phosphors [44]. Conversely, a low intense TL peak at low temperatures was observed,

15227243, 2023, 5, Downloaded from https://analyticalsciencejournals.onlinelibrary.wiley.com/doi/10.1002/bio.4488 by Sungkyunkwan University, Wiley Online Library on [16/08/2023]. See the Terms and Conditions (https://onlinelibrary.wiley.com/terms-and-conditions) on Wiley Online Library for rules of use; OA articles are governed by the applicable Creative Commons License

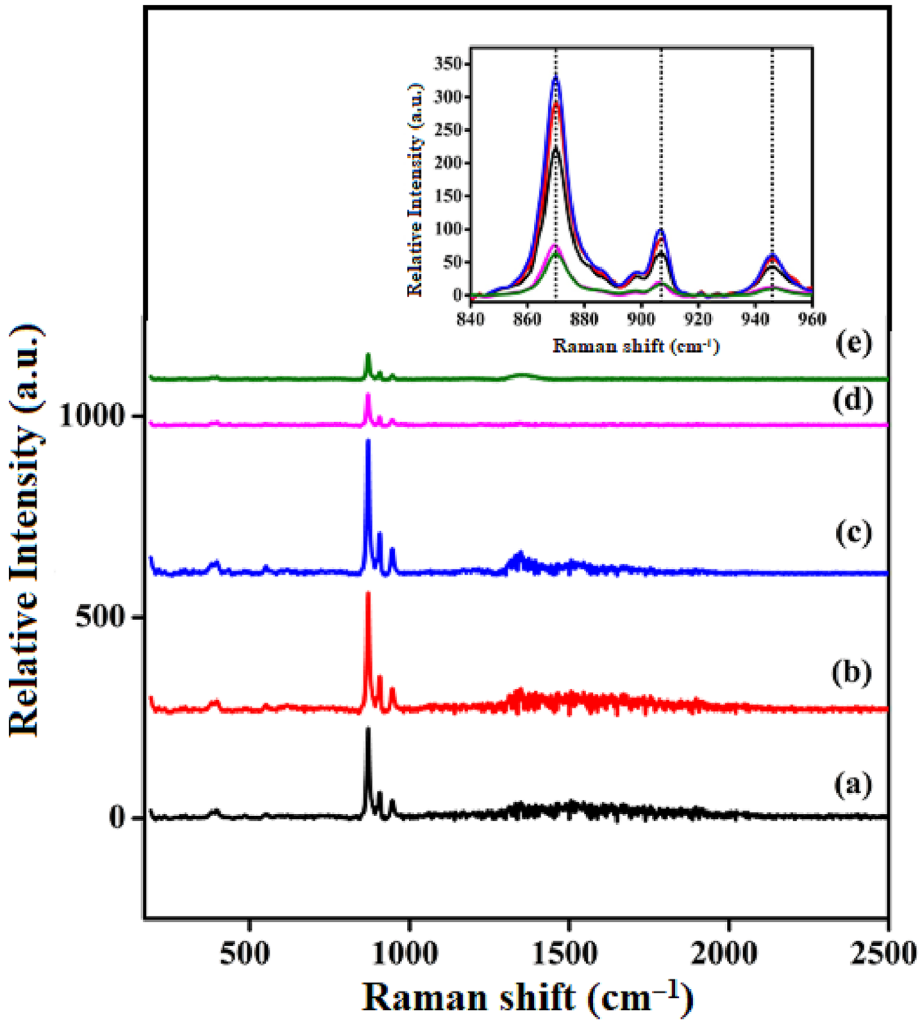

FIGURE 5 Raman spectra of the Zn_2SiO_4 materials calcinated at (curve a) 700°C, (curve b) 800°C, (curve c) 900°C, (curve d) 1000°C, and (curve e) 1100°C.

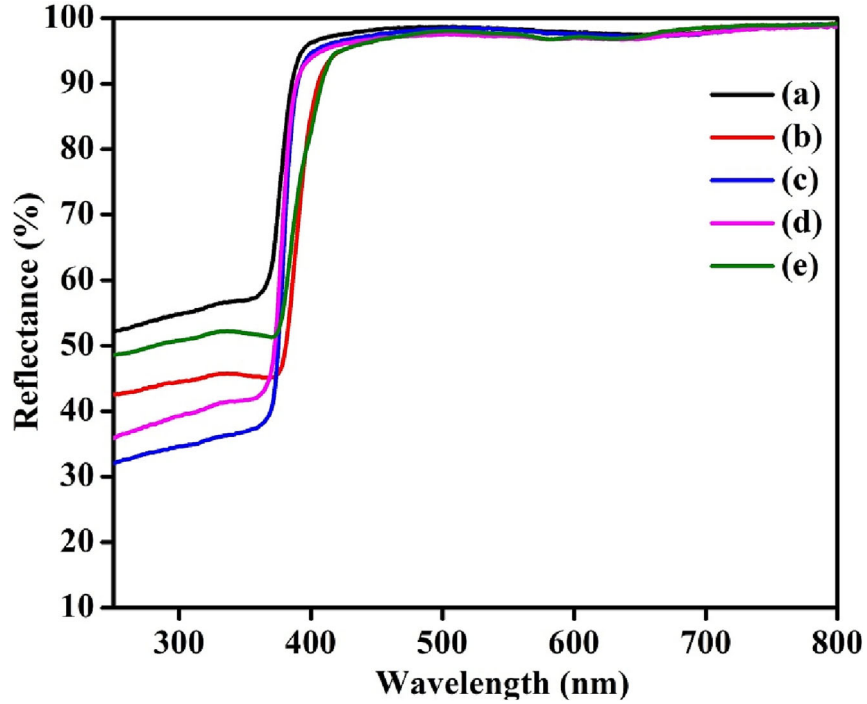

FIGURE 6 Diffuse reflectance spectra of the Zn_2SiO_4 materials calcinated at (curve a) 700°C, (curve b) 800°C, (curve c) 900°C, (curve d) 1000°C, and (curve e) 1100°C.

15227243, 2023, 5, Downloaded from https://analyticalsciencejournals.onlinelibrary.wiley.com/doi/10.1002/bio.4488 by Sungkyunkwan University, Wiley Online Library on [16/08/2023]. See the Terms and Conditions (https://onlinelibrary.wiley.com/terms-and-conditions) on Wiley Online Library for rules of use; OA articles are governed by the applicable Creative Commons License

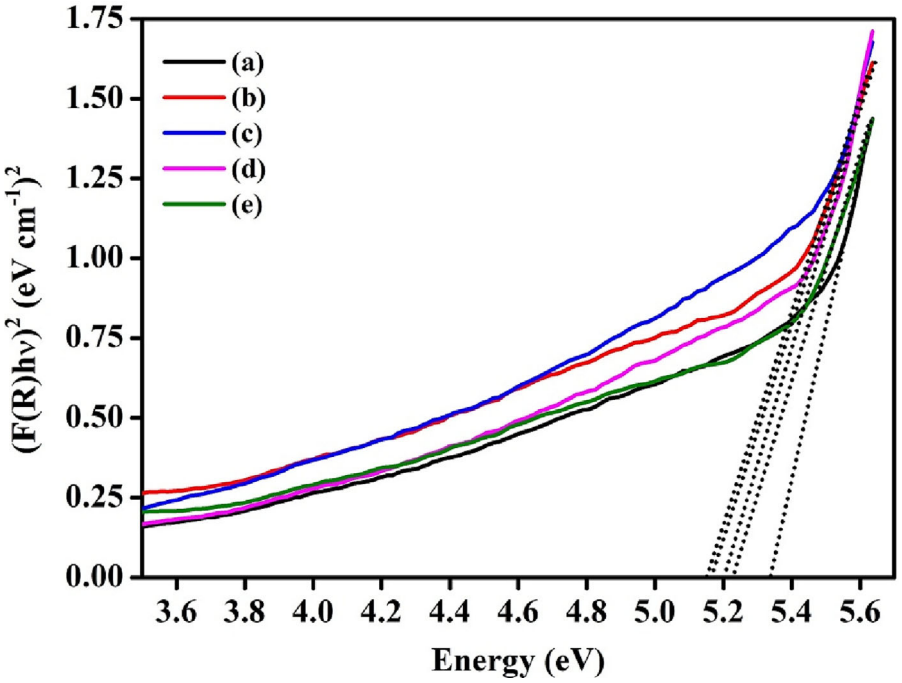

FIGURE 7 Energy band gap sof the Zn_2SiO_4 materials calcinated at (curve a) 700°C, (curve b) 800°C, (curve c) 900°C, (curve d) 1000°C, and (curve e) 1100°C.

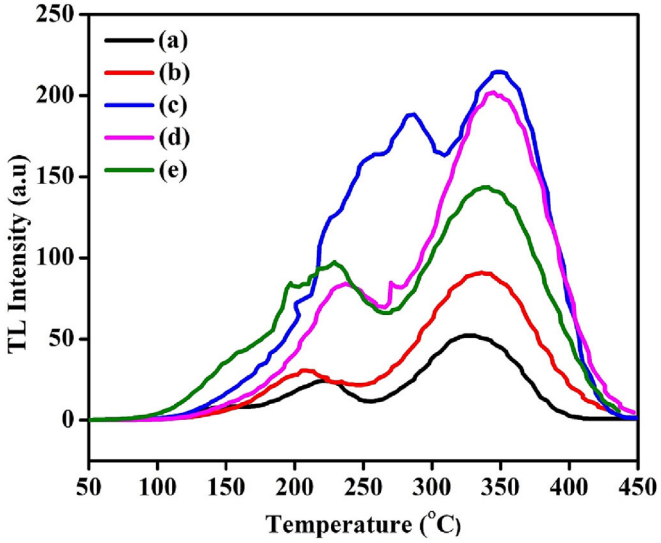

FIGURE 8 TL spectra of the Zn_2SiO_4 materials calcinated at (curve a) 700°C, (curve b) 800°C, (curve c) 900°C, (curve d) 1000°C, and (curve e) 1100°C.

TABLE 3 Peak positions of TL glow peaks for Zn_2SiO_4 materials.

	TL glow peak position (°C)	
Calcination temperature (°C)	Peak 1	Peak 2
700	223	327
800	207	335
900	285	354
1000	237	346
1100	228	337

which was likely to fade faster due to the shallower traps. In TL performance, the most satisfactory and favourable results were obtained for the Zn_2SiO_4 phosphor calcinated at 900°C. As seen in Figure 8, the Zn_2SiO_4 sample calcinated at 900°C produced two highly intense peaks at 282°C and 354°C. Furthermore, peaks 1 and 2 exhibited a peak shift towards higher temperatures, suggesting the presence of deep traps in the prepared sample, and thus showing enhanced dosimetric behaviour [44].

In general, crystallinity due to the calcination temperature plays a vital role in the generation of trap centres. Therefore, the calcination temperature needs to be optimized for stable and efficient TL characteristics. In the present study, a higher number of trapping/luminescence centres in the host system were observed in the sample calcinated at 900°C, indicating favourable TL behaviour in the Zn_2SiO_4 phosphors. Further studies in TL, such as dose–response and trapping parameters for the optimized Zn_2SiO_4 phosphor calcinated at 900°C are discussed in the next section.

3.6.1 | TL dose–response

The Zn_2SiO_4 phosphor calcinated at 900°C was irradiated with various X-ray doses to evaluate the TL glow curve [44]. The linear response of the TL glow curve was observed for various radiation doses, as shown in Figure 9. Two dosimetric peaks at 282°C and 354°C were observed; there is no change in the position of the TL peak, whereas TL intensity varied with the X-ray dose. TL glow curve intensity increased linearly with the X-ray exposure value from 0.3 Gy to 0.7 Gy. The difference in the intensity value of each curve was mainly due to the creation of some luminescence centres (LC)/trapping centres (TC), depending on the radiation dose. Limited electron

15227243, 2023, 5, Downloaded from https://analyticalsciencejournals.onlinelibrary.wiley.com/doi/10.1002/bio.4488 by Sungkyunkwan University, Wiley Online Library on [16/08/2023]. See the Terms and Conditions (https://onlinelibrary.wiley.com/terms-and-conditions) on Wiley Online Library for rules of use; OA articles are governed by the applicable Creative Commons License

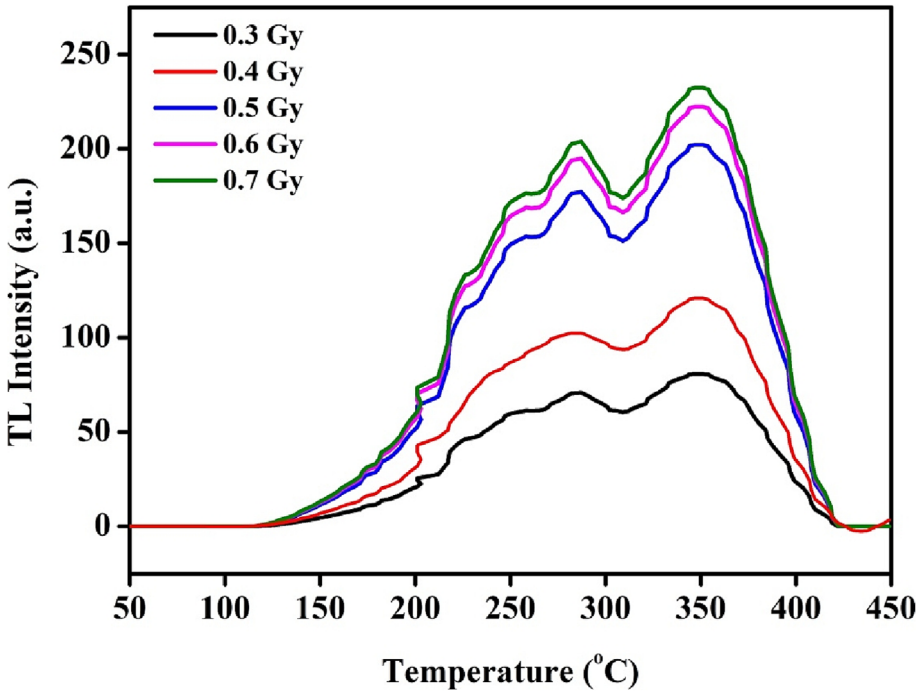

FIGURE 9 TL dose variations of the Zn_2SiO_4 material calcinated at 900°C.

and hole traps were formed at low radiation dosage. The recombination process occurred within the track. However, a further increase in the dose value reduced the space between electron–hole pair traps and additional overlapping tracks were also formed. At one end, numbers of available traps were saturated with further increase in the dose value, causing TL intensity saturation [45]. The above discussion of TL peak linearity and saturation has been described previously using the Defect Interaction Model (DIM) and Track Interaction Model (TIM) [46–48].

Overall, the population of defects/trap centres generated in a material increases with the increase in the dose value until it becomes saturated.

3.6.2 | Calculation of trapping parameters

Trapping parameters and trap levels can be analyzed from the TL glow curve. The kinetic parameters significantly affected the phosphor's dosimetric properties. Deconvolution is commonly used to examine the TL curve and study the trap characteristics. The peak shape (PS) method is well known for analyzing TL mechanisms of multiple peak luminance curves. After the sample is irradiated, electrons inside the material are trapped at distinct levels. During TL, the trapped electrons recombine and emit light. In this study, activation energy (E) and order of kinetics (b), the two essential parameters showing the stability of the luminescence trap/centre, were evaluated using the PS method. Activation energy is the energy value needed to release the trapped electrons. Information about the re-trapping of the trapped charge carriers during heating can be obtained from the order of kinetics value [49, 50]. The activation energy (E) of the trapped level in the phosphor material depends greatly on the geometry and shape of the glow curve. Kinetic parameters, such as activation energy and order of kinetics of the Zn_2SiO_4 phosphor, were calculated using the PS method for the observed glow peak acquired at the 0.57 Gy X-ray irradiation dose. The PS method is also referred to as the Chen method. The glow curves were deconvoluted using ORIGIN 8.5 software [51], as shown in Figure 10a,b. In Figure 10, ω represents the FWHM of the deconvoluted peak, the half-width of the peak on the left side is denoted as τ, and the half-width of the peak on the right side is indicated as δ. The value of the geometric form factor μ_g can be used to predict the order of kinetics for the TL glow peak. The following equation determines the value of μ_g [44]:

$$\mu_g = \frac{\delta}{\omega} \qquad (2)$$

For first-order kinetics, the value of μ_g is 0.42, while for second-order kinetics, μ_g is 0.52. The number indicates general order kinetics if it lies within the 0.42–0.52 range. The form factor μ_g value in this work was estimated to be 0.49 for peak 1 and 0.46 for peak 2, indicating that the TL glow peak kinetic order was between 1 and 2, which is regarded as a general order of kinetics [44, 52].

The activation energy E was calculated using the following equation proposed by Chen [44, 53]:

$$E = 2kT_m \frac{1.76T_m}{\omega - 1}$$

where k is Boltzmann's constant $\left(8.6 \times 10^{-5} eV K^{-1}\right)$ and T_m is the glow peak temperature corresponding to the maximum TL intensity:

15227243, 2023, 5, Downloaded from https://analyticalsciencejournals.onlinelibrary.wiley.com/doi/10.1002/bio.4488 by Sungkyunkwan University, Wiley Online Library on [16/08/2023]. See the Terms and Conditions (https://onlinelibrary.wiley.com/terms-and-conditions) on Wiley Online Library for rules of use; OA articles are governed by the applicable Creative Commons License

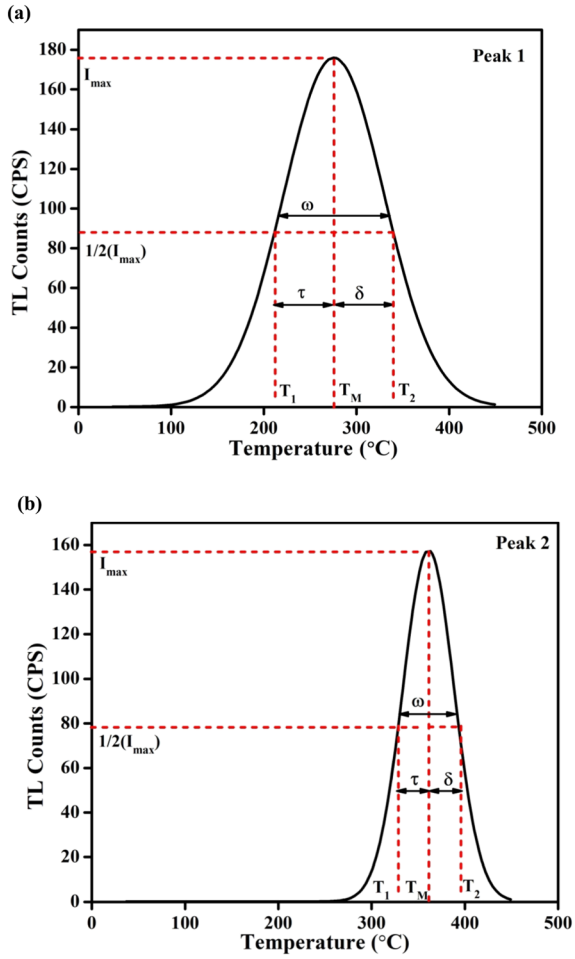

FIGURE 10 Deconvoluted TL glow curve of the Zn_2SiO_4 phosphor irradiated with 0.57 Gy X-ray irradiation. (a) Peak 1 and (b) peak 2.

$$\omega = T_2 - T_1$$

The calculated activation energy E was 0.182 eV for peak 1 and 0.634 eV for peak 2. The calculated value of the order of kinetics and the activation energy of the TL glow peaks of the synthesized Zn_2SiO_4 phosphor was more comparable with reports in previous literature, which implied that the synthesized Zn_2SiO_4 phosphor was a potential candidate for TLD applications.

4 | CONCLUSION

In conclusion, the Zn_2SiO_4 phosphor was synthesized using a hydrothermal approach with different calcination temperatures. Various analytical and spectroscopical techniques were used to examine the structural, morphology, optical, and luminescence properties of the Zn_2SiO_4 phosphor. The optimization glow curve confirmed the most suitable TL glow curve at 282°C and 354°C for the Zn_2SiO_4 phosphor calcinated at 900°C compared with other materials. The TL intensity increased linearly for both TL peaks with an increase in X-ray dose from 0.3 Gy to 0.7 Gy. The activation energy E was calculated for both high-temperature TL peaks as 0.182 eV for peak 1 and 0.634 eV for peak 2; the order of kinetics of the Zn_2SiO_4 phosphor revealed that the synthesized Zn_2SiO_4 was a favourable candidate for dosimetry applications.

AUTHOR CONTRIBUTIONS

P. Diana, D. Sivaganesh, S. Sebastian, L. Sangeetha, V. Sivakumar, S. Saravanakumar: Investigation, Methodology, Conceptualization, Experimental Design, Data curation, Formal analysis, Software Analysis. S. Saravanakumar, V. Sivakumar, Vijayendran K. K. Praneeth, Padmanathan Karthick Kannan: Writing – original draft. S. Saravanakumar, Yang Li, Ji-Man Kim, Padmanathan Karthick Kannan: Project administration, Validation, Visualization, Writing – review & editing.

ACKNOWLEDGEMENTS

One of the authors, P.D., would like to thank the Kalasalingam Academy of Research and Education (KARE) for providing a University Research Fellowship (URF) and also thank the KARE International Research Centre (IRC) for providing the instrumentation. We thank Arunachalam Lakshmanan, Dean of Research, Saveetha Engineering College, for the help rendered while recording the TL measurements. All authors would like to acknowledge Naidu Dhanpal Jayram, Plasmonic Laboratory, Department of Physics, KARE for using the Raman characterization. One of authors D. Sivaganesh, greatfully acknowledges the Ministry of Science and Higher Education of the Russian Federation (Ural Federal University, Young Scientist Competition Program-2030) for supporting his research work.

CONFLICT OF INTEREST STATEMENT

There is no conflict of interest in the present work.

DATA AVAILABILITY STATEMENT

Data will be made available on request.

ORCID

Subramanian Saravanakumar https://orcid.org/0000-0003-1406-9589
S. Sebastian https://orcid.org/0000-0002-9268-2621

REFERENCES

[1] C. Aparna, P. K. Shetty, M. G. Mahesha, *Mater. Sci. Semicond. Process.* **2022**, *150*, 106931.
[2] F. N. Flakus, *Iaea Bull.* **1981**, *23*, 31.
[3] A. Vidya Saraswathi, N. S. Prabhu, K. Naregundi, M. I. Sayyed, M. S. Murari, A. H. Almuqrin, S. D. Kamath, *Mater. Chem. Phys.* **2022**, *281*, 125872.
[4] P. P. Kulkarni, K. H. Gavhane, M. S. Bhadane, V. N. Bhoraskar, S. S. Dahiwale, S. D. Dhole, *Mater. Adv.* **2020**, *1*, 1113.
[5] B. C. Bhatt, M. S. Kulkarni, *Defect Diffus. Forum* **2014**, *347*, 179.
[6] D. J. Daniel, O. Annalakshmi, U. Madhusoodanan, P. Ramasamy, *J. Rare Earths* **2014**, *32*, 496.
[7] N. Salah, S. S. Habib, Z. H. Khan, S. Al-Hamedi, S. P. Lochab, *J. Lumin.* **2009**, *129*, 192.

15227243, 2023, 5, Downloaded from https://analyticalsciencejournals.onlinelibrary.wiley.com/doi/10.1002/bio.4488 by Sungkyunkwan University, Wiley Online Library on [16/08/2023]. See the Terms and Conditions (https://onlinelibrary.wiley.com/terms-and-conditions) on Wiley Online Library for rules of use; OA articles are governed by the applicable Creative Commons License

[8] M. T. Jose, S. R. Anishia, O. Annalakshmi, V. Ramasamy, *Radiat. Meas.* **2011**, *46*, 1026.
[9] V. Pagonis, G. Kitis, C. Furetta, *Numerical and practical exercises in thermoluminescence*, Springer, USA **2006**.
[10] A. Souza de Oliveira, J. M. M. Buarque, L. F. C. de Oliveira, C. Soares Nascimento Jr., M. A. Schiavon, H. P. Barbosa, J. H. Faleiro, J. L. Ferrari, *Int. J. Mater. Res. Sci. Technol.* **2020**, *1*, 22.
[11] S. H. Yang, H. Y. Zhang, C. C. Huang, Y. Y. Tsai, S. M. Liao, *Appl. Phys. A: Mater. Sci. Process.* **2021**, *127*, 588.
[12] T. K. G. Rao, N. F. Cano, B. N. Silva-carrera, R. M. Ferreira, H. S. Javier-ccallata, S. Watanabe, *J. Lumin.* **2016**, *177*, 139.
[13] P. Mbule, D. Mlotswa, B. Mothudi, M. Dhlamini, *J. Lumin.* **2021**, *235*, 118060.
[14] Z. G. Portakal-Uçar, M. Oglakci, M. Yüksel, M. Ayvacıklı, N. Can, *Mater. Res. Bull.* **2021**, *133*, 111025.
[15] Z. G. Portakal-Uçar, T. Dogan, S. Akça, H. Kaynar, M. Topaksu, *Radiat. Phys. Chem.* **2021**, *181*, 109329.
[16] B. C. Babu, B. H. Rudhramadevi, S. Buddhudu, *AIP Conf. Proc.* **2014**, *1591*, 1726.
[17] M. Masjedi-Arani, M. Salavati-Niasari, *Ultrason. Sonochem.* **2016**, *29*, 226.
[18] K. Su, T. D. Tilley, M. J. Sailor, *J. Am. Chem. Soc.* **1996**, *118*, 3459.
[19] Y. C. Kang, S. B. Park, *Mater. Res. Bull.* **2000**, *35*, 1143.
[20] C. C. Diao, C. F. Yang, R. L. Wang, J. J. Lin, M. Y. Fu, *J. Lumin.* **2011**, *131*, 915.
[21] J. An, J. H. Noh, I. Cho, H. Roh, J. Y. Kim, H. S. Han, K. S. Hong, *J. Phys. Chem. C* **2010**, *114*, 10330.
[22] Physical properties and applications of polymer nanocomposites, 1st ed., (Eds: S. C. Tjong, Y.-W. Mai), Woodhead, England, **2010**.
[23] R. Peña-Garcia, Y. Guerra, B. V. M. Farias, D. M. Buitrago, A. Franco, E. Padrón-Hernández, *Mater. Lett.* **2018**, *233*, 146.
[24] H. Yang, J. Shi, M. Gong, *J. Mater. Sci.* **2005**, *40*, 6007.
[25] B. Chandra Babu, S. Buddhudu, *Phys. Procedia* **2013**, *49*, 128.
[26] The obtained band gap value was more analogous to findings detailed in a previous publication, International Center for Diffraction Data, Powder Diffraction File, JCPDS-00-037-14, **2003**.
[27] S. H. Jaafar, M. Hafiz, M. Zaid, K. A. Matori, S. Hj, A. Aziz, H. M. Kamari, S. Honda, Y. Iwamoto, Crystals **2021**, *11*, 115.
[28] M. Pal, U. Pal, J. M. G. Y. Jiménez, F. Pérez-Rodríguez, *Nanoscale Res. Lett.* **2012**, *7*, 1.
[29] A. Khorsand Zak, W. H. A. Majid, M. E. Abrishami, R. Yousefi, *Solid State Sci.* **2011**, *13*, 251.
[30] A. L. Patterson, *Phys. Rev.* **1939**, *56*, 978.
[31] A. R. Molla, A. Tarafder, B. Karmakar, *J. Mater. Sci.* **2011**, *46*, 2967.
[32] H. M. Rietveld, *J. Appl. Crystallogr.* **1969**, *2*, 65.
[33] H. M. Rietveld, *Phys. Scr.* **2014**, *8*, 098002.
[34] D. Sivaganesh, S. Saravanakumar, V. Sivakumar, R. Rajajeyaganthan, M. Arun Pandian, J. Nandha Gopal, T. K. Thirumalaisamy, *Mater. Charact.* **2020**, *159*, 110035.
[35] V. Petrícek, M. Dušek, L. Palatinus, *Zeitschrift Fur Krist.* **2014**, *229*, 345.
[36] D. Sivaganesh, S. Saravanakumar, V. Sivakumar, S. Sasikumar, J. NandhaGopal, R. Ramanathan, *Luminescence* **2021**, *36*, 99.
[37] Y. Il Kim, W. Bin Im, K. S. Ryu, K. B. Kim, Y. H. Lee, J. S. Lee, *Nucl. Instruments Methods Phys. Res. Sect. B Beam Interact. With Mater. Atoms* **2010**, *268*, 346.
[38] B. C. Babu, K. N. Kumar, B. H. Rudramadevi, S. Buddhudu, *Ferroelectr. Lett. Sect.* **2014**, *41*, 28.
[39] I. M. Alibe, K. A. Matori, H. Abdul, A. Sidek, Y. Yaakob, U. R. Id, A. M. Alibe, M. Hafiz, M. Zaid, *Molecules* **2018**, *23*, 1.
[40] K. Elghniji, A. Atyaoui, S. Livraghi, L. Bousselmi, E. Giamello, M. Ksibi, *J. Alloys Compd.* **2012**, *541*, 421.
[41] J. M. M. Buarque, D. Manzani, S. L. Scarpari, M. Nalin, S. J. L. Ribeiro, J. Esbenshade, M. A. Schiavon, J. L. Ferrari, *Mater. Res. Bull.* **2018**, *107*, 295.
[42] P. Kubelka, F. Munk, *Z. Tech. Phys.* **1931**, *12*, 593.
[43] S. S. Abdullahi, S. Güner, Y. Koseoglu, I. M. Musa, B. I. Adamu, M. I. Abdulhamid, *J. Niger. Assoc. Math. Phys.* **2016**, *35*, 241.
[44] P. P. Kulkarni, K. H. Gavhane, M. S. Bhadane, V. N. Bhoraskar, S. S. Dahiwale, S. D. Dhole, *Phys. Chem. Chem. Phys.* **2022**, *24*, 11137.
[45] M. Prokic, *Nucl. Instrum. Methods*. **1980**, *175*, 83.
[46] K. H. Gavhane, M. S. Bhadane, A. S. Bhoir, P. P. Kulkarni, B. J. Patil, V. N. Bhoraskar, S. D. Dhole, S. S. Dahiwale, *J. Alloys Compd.* **2020**, *817*, 152805.
[47] D. L. Monika, H. Nagabhushana, S. C. Sharma, B. M. Nagabhushana, R. Hari Krishna, *Chem. Eng. J.* **2014**, *253*, 155.
[48] S. P. Lochab, P. D. Sahare, R. S. Chauhan, N. Salah, R. Ranjan, A. Pandey, *J. Phys. D: Appl. Phys.* **2007**, *40*, 1343.
[49] R. K. Tamrakar, D. P. Bisen, I. P. Sahu, N. Brahme, *J. Radiat. Res. Appl. Sci.* **2014**, *7*, 417.
[50] A. J. J. Bos, *Materials (Basel)* **2017**, *10*, 1357.
[51] Origin(Pro), "8.5". OriginLab Corporation, Northampton, MA, USA, **2010**.
[52] A. M. Sadek, H. M. Eissa, A. M. Basha, G. Kitis, *J. Lumin.* **2014**, *146*, 418.
[53] D. V. Sunitha, H. Nagabhushana, S. C. Sharma, F. Singh, B. M. Nagabhushana, N. Dhananjaya, C. Shivakumara, R. P. S. Chakradhar, *J. Lumin.* **2013**, *143*, 409.

SUPPORTING INFORMATION

Additional supporting information can be found online in the Supporting Information section at the end of this article.

How to cite this article: P. Diana, S. Saravanakumar, D. Sivaganesh, V. Sivakumar, Y. Li, S. Sebastian, J.-M. Kim, P. Karthick Kannan, L. Sangeetha, V. K. K. Praneeth, *Luminescence* **2023**, *38*(5), 625. https://doi.org/10.1002/bio.4488

15227243, 2023, 5, Downloaded from https://analyticalsciencejournals.onlinelibrary.wiley.com/doi/10.1002/bio.4488 by Sungkyunkwan University, Wiley Online Library on [16/08/2023]. See the Terms and Conditions (https://onlinelibrary.wiley.com/terms-and-conditions) on Wiley Online Library for rules of use; OA articles are governed by the applicable Creative Commons License